nature nanotechnology

SUPPLEMENTARY INFORMATION

DOI: 10.1038/NNANO.2010.149

# Thermal conductivity reduction in phononic nanomesh structures

Jen-Kan Yu[#], Slobodan Mitrovic[#], Douglas Tham, Joseph Varghese and James R. Heath[*]

Division of Chemistry and Chemical Engineering, MC 127-72 1200 East California Blvd

California Institute of Technology, Pasadena CA 91125

# These authors contributed equally to this work

* email: heath@caltech.edu

## Supplemental information

### Device Fabrication

All devices were prepared on silicon-on-insulator (SOI; Soitec Inc.) wafers. The SOI wafers were pre-doped by thermally diffusing spin-on-dopant (Boron A; Filmtronics, Inc.) with rapid thermal annealing (RTA) at 820°C for 3 minutes. The resulting sheet resistance indicates a doping concentration of $2x10^{19}$ $cm^{-3}$, with the thickness of the silicon epilayer determined by atomic force microscopy to be 25 nm, 22 nm and 20 nm (depending on the device) with a variance of 1 nm. The nanomesh films (NM) and nanowires (NWA) are fabricated by the SNAP technique [30], while the e-beam nanomesh (EBM) and thin films (TF) are defined by e-beam lithography (EBL).

For the NM devices, two perpendicularly aligned Pt nanowire arrays are made using two consecutive superlattice nanowire pattern array (SNAP) procedures on top of an SOI wafer (Soitec, Inc.). SNAP protocols are described in Refs. 17 and 30. For the NWA devices only one SNAP procedure is carried out, resulting in a single, aligned Pt nanowire array. For the EBM and TF devices, e-beam lithography and metallization are used to make the transfer-ready Pt nanostructures. Next, we define the membranes

DOI: 10.1038/NNANO.2010.149

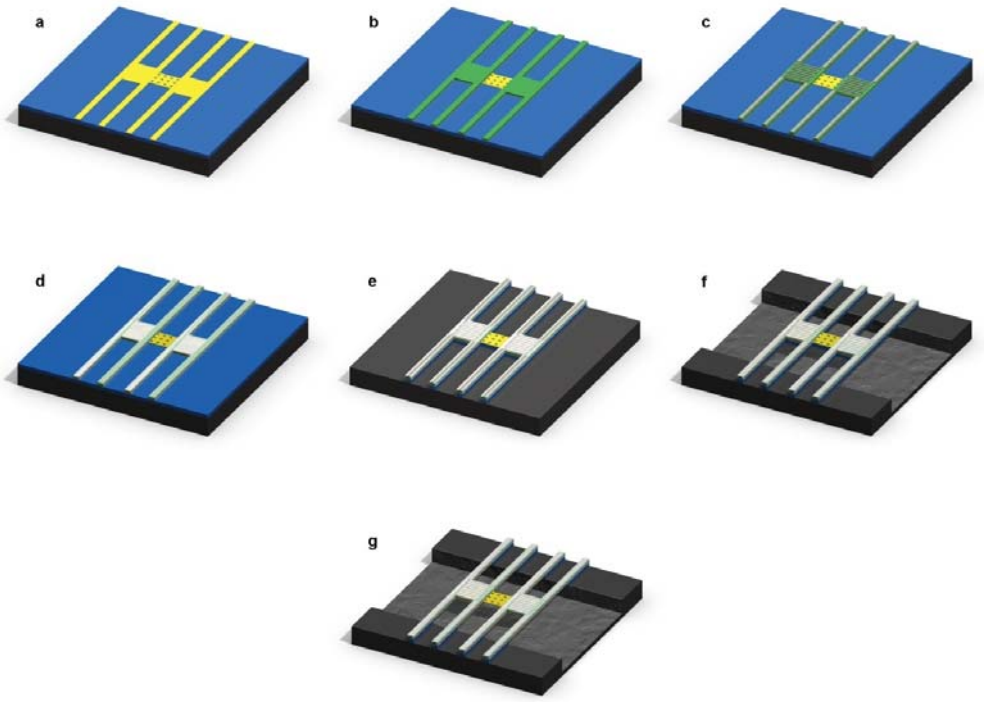


**Figure S1. Device fabrication.** The scale of the device is exaggerated from reality for better visualiztion. (a) Silicon nanomesh with monolithically-defined silicon device platform. (Yellow). (b) Device platform with silicon-nitride film as the structural backbone. (c) Ti/Pt heater/sensor defined on to the platform. (d) Parylene C conformally deposited on to the platform. (e) Buried oxide removed by RIE1 process. (f) Si handle layer etched by $XeF_2$. (g) Device fully suspended by buried oxide removal with HF vapor.

and the beams (hereafter referred to as the device platform) by electron-beam lithography and electron-beam assisted metal evaporation. The pattern transfer is performed by a $CF_4$/He reactive ion etch (hereafter referred to as RIE1). The etch is terminated at the buried oxide layer by endpoint detection via a surface reflectivity measurement. Afterwards, Pt is removed by aqua regia ($HNO_3$:HCl = 1:3) followed by 10 minutes of piranha ($H_2SO_4$:$H_2O_2$ = 5:1) cleaning. At this point, both the silicon device (NM, EBM, NWA or TF) and the silicon device platform have been made (Fig. S1a). The following steps are identical regardless of the device type (hereafter referred to as device).

An Al etch mask is placed on top of the device to protect it in subsequent fabrication step. The top few nanometers of the device platform are removed at this point by RIE1 to make it electrically insulating. A 250 nm thick low-stress silicon-nitride film, which serves as a structural backbone to the platform, is then deposited via plasma enhanced chemical vapor deposition (PECVD, STS Multiplex).

Another Al etch mask is then placed on top of the silicon-nitride layer, and patterned to match the device platform. An RIE1 process then defines the silicon-nitride film to match the shape of the platform. Al is then removed using an acidic mixture ($H_3PO_4$:$CH_3COOH$:$HNO_3$:$H_2O$ = 16:1:1:2). The resulting structure looks much the same as before, but has been greatly strengthened by silicon-nitride (Figure S1b). Next, the platinum resistive thermometers (PRT), which also serve as heaters, are fabricated by EBL and metallization - typically, 60 nm of Pt is deposited on top of a 10 nm Ti adhesion layer (Figure S1c).

Device suspension involves the gas phase etchants $XeF_2$ and HF vapor. The device platform is protected from damage by the HF vapor by a 200 nm layer of poly(monochloro-*p*-xylylene) or parylene C (SCS parylene deposition system). Parylene C coating has proven to be conformal, pinhole free and resistive to HF [31]. Prior to parylene coating, an Al metal mask was deposited onto the device to prevent direct contact with parylene. Similarly, another metal etch-mask, Al or Ni-Cr, is placed on top of the parylene layer and over the device platform. $O_2$ plasma (RIE, Unaxis) is then used to etch through parylene, and results in a structure that is now protected from HF vapor damage (Figure S1d). [32]. It is necessary to also etch through the buried oxide layer and reach the underlying Si handle layer. This is to facilitate the removal of the buried oxide under the device in order to achieve a fully suspended device. RIE1 etch is again used to etch through the oxide, stopping once the handle layer has been reached (Figure S1e). As before, an Al film was protecting the device, including the platform, from etching. After the removal of Al, the device and the platform are ready for suspension.

A layer of 6% polymethyl methacrylate (PMMA) e-beam resist is spun on the chip, and two openings in PMMA are patterened on each side of the device platform. $XeF_2$ etch (custom $XeF_2$ pulsed etching system) through the holes is isotropic and undercuts the device platform, releasing it from the chip (Figure S1f). The overall etch time is about 2 minutes at 2000 mTorr and room temperature. The PMMA layer is then removed using an acetone bath, followed by methanol, before finally drying by a $CO_2$ supercritical drying process (Automegasamdri-915B, Tousimis).

An HF vapor etch process is then applied to release the device from the buried oxide substrate, resulting in a fully suspended device (Figure S1g). A home-built HF vapor etcher equipped with a wafer

DOI: 10.1038/NNANO.2010.149

heating stage was designed for homogeneous and stiction-free oxide removal at elevated temperatures. The etching process is performed with the wafer heated to a temperature of ~80°C and exposed to the HF environment for ~30 minutes to completely remove the buried oxide layer of ~125 nm in thickness. The sample is wire-bonded to a chip that is promptly inserted into the vacuum measurement system. All measurements are performed at pressures smaller than $7\times10^{-6}$ mTorr.

**Measurement Procedure**

Li Shi et al. have detailed measurement and analysis procedures in their report of thermal and thermoelectric property measurements of one-dimensional nanostructures on suspended device platforms [18]. We adapted their platform and procedures to enable measurements of thermal conductance on monolithically-fabricated, fully-suspended devices on SOI substrates. We refer the reader to their work for details on the procedures. In the following, we briefly summarize our adaptation.

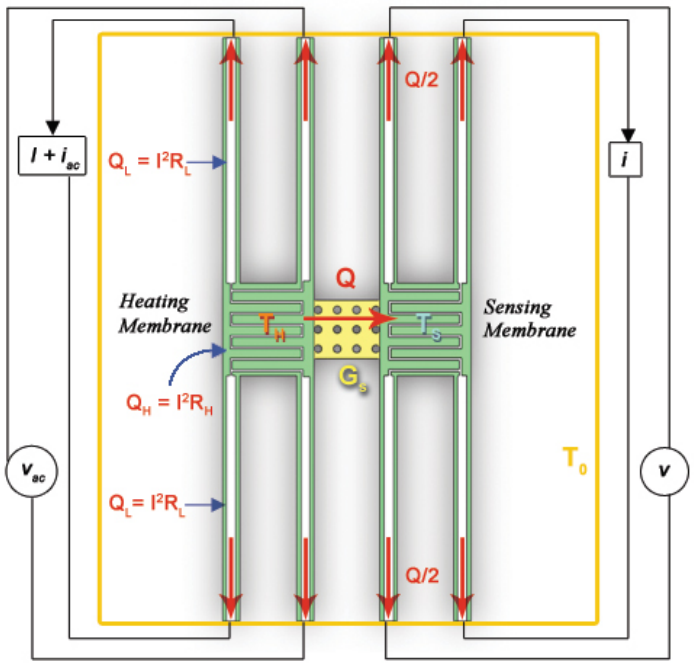


**Figure S2. Schematic diagram for the thermal conductivity measurement platform.** $T_H$ and $T_S$ represent the temperatures of the heating and sensing membranes respectively. $T_0$ is the substrate temperature. $Q_H$, $Q_L$ represents the amount of heat generated by the heater and the lead, respectively. Q is the amount of heat transported through the sample and $G_s$ is the thermal conductance of the sample.

In our measurement platform, the sample is bridged between a pair of suspended membrane "islands", as previously described in the **Device Fabrication** section. Each membrane contains a set of serpentine Pt lines that serves as a PRT and is suspended by four long (~70 $\mu$m) beams along which the electrical connections are routed.

One of the PRTs also serves as a heater and measures the hot side temperature. The other measures the cold side temperature. (Figure S2)

The cryostat is ramped to a set temperature $T_0$ at a rate of <3 K min$^{-1}$ to minimize thermal stresses on the suspended structure. After the cryostat temperature has stabilized, a current source (Keithley 6221) is used to supply a small sinusoidal current $i_{ac,h} \sim 250$ nA at frequency $f_h > 700$ Hz on top of a dc current $I$ to the heating PRT. The differential resistances $R_h$ (resistance of the serpentine element) and $R_L$ (resistance of the lead) of the heating PRT are measured simultaneously with a pair of lock-in amplifiers (Stanford Research Systems SRS830). Another SRS830 lock-in is used to source a sinusoidal current $i_{ac,s} \sim 250$ nA at frequency $f_s$ through a high-precision 10 MΩ metal film resistor (Vishay Sfernice CNS020) to the sensing PRT, while measuring the differential resistance $R_s$. These measurements are repeated for the entire set of dc currents before the cryostat is ramped to another set temperature, upon which the measurement cycle repeats.

At the conclusion of the experiment, the set of $R_s(I=0)$ and $R_h(I=0)$ acquired at various temperatures $T_0$ is fitted using linear least squares regression to obtain $\mathrm{d}R_s(I=0)/\mathrm{d}T$ and $\mathrm{d}R_h(I=0)/\mathrm{d}T$. The temperature rise of the heating and sensing PRTs are then given as

$$\Delta T_h = \frac{\Delta R_h(I)}{\dfrac{dR_h(I=0)}{dT}}; \qquad \Delta R_h = R_h(I) - R_h(I=0) \qquad \text{for} \qquad f_h > 700 \text{ Hz}$$

$$\Delta T_s = \frac{\Delta R_s(I)}{\dfrac{dR_s(I=0)}{dT}}; \qquad \Delta R_s = R_s(I) - R_s(I=0)$$

The Joule heat developed in the heating PRT and its leads are $Q_h = I^2 R_h$ and $2Q_L = 2I^2 R_L$ and we can thus calculate the beam and sample thermal conductances.

$$G_b = \frac{Q_h + Q_L}{\Delta T_h + \Delta T_s}$$

$$G_s = G_b \frac{\Delta T_s}{\Delta T_h - \Delta T_s}$$

**Error Analysis**

DOI: 10.1038/NNANO.2010.149

We have adopted the procedures described by Li Shi et al [18] and begin our data analysis by calibrating the resistances of the PRTs on each membrane as a function of T. We then apply a dc heating current to one of the PRTs to cause Joule heating of that membrane. This results in a temperature difference between the membranes, and heat is dissipated through the bridging sample. Finally, the sample thermal conductance is evaluated with the known magnitude of the Joule heat and the measured temperature difference.

The platinum resistance thermometers (PRTs) are calibrated by linear least squares fitting of the PRT resistances at $I = 0$ to polynomial functions of the membrane temperature. Two conditions must be met for this fit to be valid. When the heating PRT is "off" (i.e., dc current $I = 0$), we assume both membranes to be at the same temperature $T$, equal to the environment temperature $T_0$. This approximation is excellent only if the lock-in excitation ac currents $i_{ac,h}$ and $i_{ac,s}$ are chosen to be small (~250 nA), so that their heating contributions can be neglected. Second, because linear least squares analysis implicitly assumes the independent variable $T$ to be error-free, the random errors in the resistance must dominate. Typically, measurement noise in the environment temperature $T_0$ is <25 mK at 100–300 K (<0.025%), while the resistance errors are generally ~1%. As the random errors in our $T$ measurements are more than an order of magnitude smaller than those in $R$, we may safely use linear least squares fitting. Figure 3 shows a typical fit for the heating PRT resistance. We note that the residuals are on the order of no more than ~0.3%.

In the following, we will first focus on the derivation of the "fitting error" introduced by the use of linear least squares fitting to a model function. Later, measurement errors are considered. Both sources of error are propagated into a final estimate for the random error in the sample thermal conductance $G_s$. Finally, we highlight a potential source of systematic error and explain how it can be eliminated.

*Random errors in the fit coefficients $\beta_n$*

The random error in the polynomial fit coefficients is by far the most onerous to obtain and we will derive it explicitly here. For the sake of clarity, we will momentarily set aside the distinction between the heating and sensing PRTs in the following discussion. Let us initially consider a linear fit for the

resistance $R(T) = \beta_1 + \beta_2 T$, where $\beta_1$ and $\beta_2$ are fit coefficients to be determined. Assume that we have performed single-shot measurements of the couple ($T_i$, $R_i$) at each of $i = 1,\ldots,m$ different temperatures. (We consider multiple measurements at the end of this section.)

Let us define a residual function $r_i$ for each of the $m$ data point ($T_i$, $R_i$) as

$$r_i = R_i - (\beta_1 + \beta_2 T_i) \qquad \text{for } i = 1,\ldots,m.$$

The goal of linear least squares is to minimize the sum of squares $S$

$$S = \sum_{i=1}^{m} W_{ii} r_i^2$$

of the residual $r_i$, weighted by the weight factor $W_{ii}$. The minimum of $S$ is found with the minimization conditions

$$\left.\begin{aligned} \frac{\partial S}{\partial \beta_1} = 0 = 2\sum_{i=1}^{m} W_{ii} r_i \frac{\partial r_i}{\partial \beta_1} \\ \frac{\partial S}{\partial \beta_2} = 0 = 2\sum_{i=1}^{m} W_{ii} r_i \frac{\partial r_i}{\partial \beta_2} \end{aligned}\right\} \Rightarrow \begin{aligned} \sum_{i=1}^{m} W_{ii} r_i (\beta_1 + \beta_2 T_i) = \sum_{i=1}^{m} W_{ii} R_i \\ \sum_{i=1}^{m} W_{ii} r_i (\beta_1 + \beta_2 T_i) T_i = \sum_{i=1}^{m} W_{ii} R_i T_i \end{aligned}$$

and we can rewrite the minimization conditions as a matrix

$$\begin{bmatrix} 1 & \cdots & m \\ T_1 & \cdots & T_m \end{bmatrix} \begin{bmatrix} W_{11} & \cdots & 0 \\ \vdots & \ddots & \vdots \\ 0 & \cdots & W_{mm} \end{bmatrix} \begin{bmatrix} 1 & T_1 \\ \vdots & \vdots \\ m & T_m \end{bmatrix} \begin{bmatrix} \beta_1 \\ \beta_2 \end{bmatrix} = \begin{bmatrix} 1 & \cdots & m \\ T_1 & \cdots & T_m \end{bmatrix} \begin{bmatrix} W_{11} & \cdots & 0 \\ \vdots & \ddots & \vdots \\ 0 & \cdots & W_{mm} \end{bmatrix} \begin{bmatrix} R_1 \\ \vdots \\ R_m \end{bmatrix}$$

or more concisely in vector notation

$$\mathbf{T}^{\mathrm{T}}\mathbf{W}\mathbf{T}\beta = \mathbf{T}^{\mathrm{T}}\mathbf{W}\mathbf{R}$$

where $\boldsymbol{\beta}$ is the vector of fit coefficients, $\mathbf{R}$ the resistance vector, $\mathbf{W}$ the (diagonal) weight matrix and $\mathbf{T}$ the temperature matrix. This result is general for any order of the polynomial fit.

Rearranging the result above, we obtain

$$\beta = (\mathbf{T}^{\mathrm{T}}\mathbf{W}\mathbf{T})^{-1}\mathbf{T}^{\mathrm{T}}\mathbf{W}\mathbf{R} \quad \textbf{--- Eq(1)}$$

which enables the estimation of the errors in the fit coefficients that arise from non-zero residuals in fitting the $R_i$ points. In other words, given a covariance matrix $\mathbf{M}$ of the resistance vector $\mathbf{R}$, and **Eq(1)** above, the covariance matrix $\mathbf{M}^{\boldsymbol{\beta}}$ of the fit coefficients $\boldsymbol{\beta}$ is

DOI: 10.1038/NNANO.2010.149

$$\mathbf{M}^{\beta} = (\mathbf{T}^{\mathrm{T}}\mathbf{W}\mathbf{T})^{-1}\mathbf{T}^{\mathrm{T}}\mathbf{W}\mathbf{M}\mathbf{W}^{\mathrm{T}}\mathbf{T}(\mathbf{T}^{\mathrm{T}}\mathbf{W}\mathbf{T})^{-1}$$

from the mapping property of covariance matrices.

Assuming the measurement errors are uncorrelated, the covariance matrix of $\mathbf{R}$ is given as $\mathbf{M} = \sigma^2\mathbf{I}_n$ where $\mathbf{I}_n$ is the $n\times n$ identity matrix and $\sigma^2$ is the variance of the residual $r_i$, estimated from

$$\sigma^2 = \sum_{i=1}^{m} \frac{r_i^2}{m-n}$$

where $n$ is the number of fit coefficients (e.g., $n = 2$ for a linear fit: $\beta_1$ and $\beta_2$). For uncorrelated errors, we use unit weights for all points ($\mathbf{W} = \mathbf{I}_m$, the $m\times m$ identity matrix), so that

$$\mathbf{M}^{\beta} = (\mathbf{T}^{\mathrm{T}}\mathbf{M}^{-1}\mathbf{T})^{-1} = \sigma^2(\mathbf{T}^{\mathrm{T}}\mathbf{T})^{-1}.$$

For the explicit example of $n = 2$ (straight-line) fitting, we obtain

$$\mathbf{M}^{\beta} = \frac{\sigma^2}{m\sum T_i^2 - (\sum T_i^2)^2}\begin{bmatrix} \sum T_i^2 & -\sum T_i \\ -\sum T_i & m \end{bmatrix} \text{ and } \sigma^2 = \sum \frac{r_i^2}{m-2}.$$

The variances in the fit coefficients $\beta_1$ and $\beta_2$ can be read off directly as

$$\sigma_{\beta_1}^2 = \mathbf{M}_{11}^{\beta} = \frac{\sigma^2\sum T_i^2}{m\sum T_i^2 - (\sum T_i)^2}$$

$$\sigma_{\beta_2}^2 = \mathbf{M}_{22}^{\beta} = \frac{m\sigma^2}{m\sum T_i^2 - (\sum T_i)^2}$$

which are the standard results.

In the general case of the $(n-1)^{\text{th}}$-order polynomial fitting with $n$ fit coefficients, we obtain

$$\mathbf{M}^{\beta} = \sigma^2\begin{bmatrix} m & \sum T_i & \cdots & \sum T_i^n \\ \sum T_i & \sum T_i^2 & \cdots & \sum T_i^{n+1} \\ \vdots & \vdots & \ddots & \vdots \\ \sum T_i^n & \sum T_i^{n+1} & \cdots & \sum T_i^{2n} \end{bmatrix}^{-1} \text{ and } \sigma^2 = \sum \frac{r_i^2}{m-n}.$$

We conclude this section by considering the impact of making $j = 1,\ldots,N$ multiple measurements of $R_i$ and $T_i$ at each of $m$ different temperatures ($i = 1,\ldots,m$). The preceding results are simply modified with replacement of the variables $R_i$ and $T_i$ by their mean values

$$R_i \mapsto \overline{R_i} = \frac{1}{N}\sum_{j=1}^{N} R_i \text{ and } T_i \mapsto \overline{T_i} = \frac{1}{N}\sum_{j=1}^{N} T_i .$$

The variance of residuals $\sigma^2$ should be interpreted as the "fitting error" and is a measure of how well the fit function $R(T)$ fits the measured points. It depends primarily on the fitting function used and is only partly affected by measurement error. Hence we leave it unmodified. Therefore, a proper choice of the fitting function is crucial if the errors in the fit coefficients are to be minimized.

*Random error in the gradient dR/dT*

The slope $dR/dT$ is required for determination of the membrane temperature from the PRT resistance measurements. In this section, we will obtain an error estimate for the slope, given the error estimates for the fit coefficients derived in the preceding section. For a polynomial function of order $(n-1)$ with $n$ fit coefficients

$$R(T) = \beta_1 + \beta_2 T + \ldots + \beta_n T^{n-1}$$

the slope is

$$\frac{dR}{dT} = \beta_2 + 2\beta_3 T + \ldots + (n-1)\beta_n T^{n-2}.$$

A popular fit for platinum resistance thermometers is the Callendar-Van Dusen equation

$$R(T) = R_0[1 + AT + BT^2 + CT^3(T-100)]$$

which suggests a polynomial fit of up to 4$^{th}$-order. In our analyses, we have found a 3$^{rd}$-order polynomial fit sufficiently accurate, with little discernable reduction in the residuals for higher orders. Therefore, we will explicitly derive the error in the slope for cubic polynomial fits below.

The slope of a cubic polynomial fit is

$$\frac{dR}{dT} = \beta_2 + 2\beta_3 T + 3\beta_4 T^2$$

and therefore an estimate of the variance of the slope is

DOI: 10.1038/NNANO.2010.149

$$\sigma^2_{\frac{dR}{dT}} \approx \underbrace{\sigma^2_{\beta_2} + 4T^2\sigma^2_{\beta_3} + 9T^2\sigma^2_{\beta_4}}_{\text{variance terms}} + \underbrace{4T\sigma_{\beta_2\beta_3} + 6T^2\sigma_{\beta_2\beta_4} + 12T^3\sigma_{\beta_3\beta_4}}_{\text{covariance terms}}$$

$$= \overbrace{\mathbf{M}^{\beta}_{22} + 4T^2\mathbf{M}^{\beta}_{33} + 9T^4\mathbf{M}^{\beta}_{44}} + \overbrace{4T\mathbf{M}^{\beta}_{23} + 6T^2\mathbf{M}^{\beta}_{24} + 12T^3\mathbf{M}^{\beta}_{34}}$$

We have dropped variance and covariance terms involving the independent variable $T$, as it is assumed to be error-free. It is necessary to keep all remaining covariance terms: the fit coefficients are correlated, even if the measurements are not.

For all other fit orders, we provide the estimated variance of the slope in vector notation, again neglecting (co)variance in $T$,

$$\sigma^2_{\frac{dR}{dT}} \approx \mathbf{A}^{\mathrm{T}}\mathbf{M}^{\beta}\mathbf{A} \text{ where } \mathbf{A}^{\mathrm{T}} = \begin{bmatrix} 0 & 1 & 2T & \cdots & nT^{n-1} \end{bmatrix}$$

if all variance and covariance terms are kept and

$$\sigma^2_{\frac{dR}{dT}} \approx \mathrm{Tr}\left[\mathbf{A}^{\mathrm{T}}\mathbf{M}^{\beta}\mathbf{A}\right] \text{ where } \mathbf{A}^{\mathrm{T}} = \begin{bmatrix} 0 & & & & \\ & 1 & & & \\ & & 2T & & \\ & & & \ddots & \\ & & & & nT^{n-1} \end{bmatrix}$$

if only the variance terms are desired.

*Random error in the temperature rise ΔT*

Following the analysis of Li Shi *et al*, the temperature rise is given by

$$\Delta T_h = \frac{R_h(I) - R_h(I=0)}{\frac{dR_h(I=0)}{dT}} \text{ for } f_h >> 1/2\pi\tau \sim 100 \text{ Hz}$$

for the heating PRT, where $\tau$ is the thermal time constant of the suspended device. We use this form as we perform our measurements at $f_h \sim 1$ kHz. The expression is

$$\Delta T_s = \frac{R_s(I) - R_s(I=0)}{\frac{dR_s(I=0)}{dT}}$$

for the sensing PRT. $R_s(I)$ and $R_s(I=0)$ respectively denote the measured values of resistance $R_s$ with and without a dc current flowing in the heating PRT. From the preceding discussion, assuming uncorrelated errors in the resistance measurements, we obtain for the estimated variance in the temperature rise

$$\sigma^2_{\Delta T_{h,s}} = \left[\left(\frac{\sigma_{R_{h,s}(I)}}{R_{h,s}(I)} + \frac{\sigma_{dR_{h,s}/dT}}{dR_{h,s}/dT}\right)\frac{R_{h,s}(I)}{dR_{h,s}/dT}\right]^2 + \left[\left(\frac{\sigma_{R_{h,s}(I=0)}}{R_{h,s}(I=0)} + \frac{\sigma_{dR_{h,s}/dT}}{dR_{h,s}/dT}\right)\frac{R_{h,s}(I=0)}{dR_{h,s}/dT}\right]^2$$

where the subscripts *h,s* denote heating and sensing PRTs respectively.

The (differential) resistances $R_h$, $R_L$ and $R_s$ are obtained from the raw lock-in voltage measurements on the inner and outer electrodes of each PRT, using the following equations

$$\left.\begin{aligned} R_h^{outer} &= \frac{v_{ac,h}^{outer}}{i_{ac,h}} \\ R_h^{inner} &= \frac{v_{ac,h}^{inner}}{i_{ac,h}} \\ R_s^{outer} &= \frac{v_{ac,s}^{outer}}{i_{ac,s}} \\ R_s^{inner} &= \frac{v_{ac,s}^{inner}}{i_{ac,s}} \end{aligned}\right\} \Rightarrow \begin{aligned} R_h &= R_h^{inner} \\ R_L &= R_h^{outer} - R_h^{inner} \\ R_s &= R_s^{inner} \end{aligned}$$

and assuming uncorrelated measurement errors, the variances are

$$\sigma^2_{R_h} = R_h^2\left[\left(\frac{\sigma_{v_{ac,h}^{inner}}}{v_{ac,h}^{inner}}\right)^2 + \left(\frac{\sigma_{i_{ac,h}}}{i_{ac,h}}\right)^2\right]$$

$$\sigma^2_L = R_L^2\left\{\left(R_h^{outer}\right)^2\left[\left(\frac{\sigma_{v_{ac,h}^{outer}}}{v_{ac,h}^{outer}}\right)^2 + \left(\frac{\sigma_{i_{ac,h}}}{i_{ac,h}}\right)^2\right] + \left(R_h^{inner}\right)^2\left[\left(\frac{\sigma_{v_{ac,h}^{inner}}}{v_{ac,h}^{inner}}\right)^2 + \left(\frac{\sigma_{i_{ac,h}}}{i_{ac,h}}\right)^2\right]\right\}$$

$$\sigma^2_{R_s} = R_s^2\left[\left(\frac{\sigma_{v_{ac,s}^{inner}}}{v_{ac,s}^{inner}}\right)^2 + \left(\frac{\sigma_{i_{ac,s}}}{i_{ac,s}}\right)^2\right]$$

We estimate the random error in $v_{ac}$ ("inner" and "outer" for both heating and sensing PRTs) using either the sample variance of the measured voltages, or the reading error from the vendor datasheet, whichever is larger. We have calibrated the heating PRT current source (see section on systematic errors below) and estimate the error in $i_{ac,h}$ with the calibration reading error. We used a resistor (Vishay Sfernice CNS020)

DOI: 10.1038/NNANO.2010.149

to convert a voltage source (Stanford Research Systems SRS830) into a current source for the sensing PRT, so the random error in $i_{ac,s}$ includes both resistor and instrumental contributions.

*Random errors in the Joule heats $Q_h$ and $Q_L$*

The Joule heat dissipated by the passage of a dc current $I$ is $Q_h = I^2R_h$ in the heating PRT, and $2Q_L = 2I^2R_L$ in the pair of current-carrying leads. Assuming uncorrelated measurement errors, the variance is

$$\sigma_{Q_{h,L}}^2 = Q_{h,L}^2\left[4\left(\frac{\sigma_I}{I}\right)^2 + \left(\frac{\sigma_{R_{h,L}}}{R_{h,L}}\right)^2\right]$$

where the subscripts $h,L$ denote heating PRT and current-carrying lead respectively. The variance in $I$ is estimated from the vendor datasheets for our current source (Keithley Instruments Model 6221).

*Random errors in the thermal conductances $G_b$ and $G_s$*

The beam thermal conductance is given as

$$G_b = \frac{Q_h + Q_L}{\Delta T_h + \Delta T_s}$$

and we obtain the variance in $G_b$ as

$$\sigma_{G_b}^2 = G_b^2\left[\frac{\sigma_{Q_h}^2 + \sigma_{Q_L}^2}{(Q_h + Q_L)^2} + \frac{\sigma_{\Delta T_h}^2 + \sigma_{\Delta T_s}^2}{(\Delta T_h + \Delta T_s)^2}\right].$$

The sample thermal conductance is [18]:

$$G_s = G_b\frac{\Delta T_s}{\Delta T_h - \Delta T_s} = G_b\frac{1}{(\Delta T_h/\Delta T_s) - 1}$$

and we obtain the variance in $G_s$ as

$$\sigma_{G_s}^2 = G_s^2\left[\left(\frac{\sigma_{G_b}}{G_b}\right)^2 + \frac{\Delta T_s^2\sigma_{\Delta T_h}^2 + \Delta T_h^2\sigma_{\Delta T_s}^2}{\Delta T_s^2(\Delta T_h - \Delta T_s)^2}\right].$$

Both variances were calculated assuming uncorrelated errors in measurements.

*Systematic errors in the thermal conductance $G_s$*

We do not expect difficulties with systematic error when measurements are performed with properly calibrated instruments. Instead, we will highlight a potential source of systematic error when using our

approach. We used a Keithley Instruments Model 6221 as the current source for the heating PRT. The instrument provides a convenient way to superpose a sinusoidal ac current with amplitude $i_{ac,h}$ on top of an dc offset current $I$.

For the sinusoidal ac current $i_{ac,h}$, the vendor specifies an accuracy of 1% of $i_{ac,h}$ + 0.2% of the working range, while for the dc current $I$, the quoted accuracy is 0.2% of $I$ + 0.2% of the working range. The working range can be no smaller than the magnitude of $I + i_{ac,h}$. Because $I$ (~ 20 $\mu$A) is much larger than $i_{ac,h}$ (~ 250 nA) in our experiments, the working range error contribution affects $i_{ac,h}$ disproportionately. Even though our instrument performed well within specifications, we found a 10-20% error between the displayed value and the actual value of $i_{ac,h}$ sourced. The magnitude of the error was fixed for a given range selection, so we performed all our measurements within the same working range. To correct for the error, we measured the actual value of $i_{ac,h}$ sourced by the Model 6221, using a Stanford Research Systems SRS830 lock-in amplifier. The result is a value of $i_{ac,h}$ accurate to 1% with precision limited by the SRS830 reading error.

**Uncertainty of the Thermal Conductivity $\delta_\kappa$**

The thermal conductivity is obtained from the measured thermal conductance of each sample and the geometrical factor ($\kappa = G_s \times$ geometrical factor), i.e. the cross-section and length of the equivalent channels for the NM and EBM; and the exact cross section and length of the NWA and TF samples. The geometrical factor (G.F.) for the NWA, EBM, NM can be described by G.F. = L/(n×T×W) where L represents the length of the system across the measurement platform, n is the number of wires or equivalent channels, T is the thickness of the silicon epilayer, and W is the width of a nanowire or equivalent channel (Figure 2a). The number of nanowires can be calculated by dividing the total width of the sample $W_0$, by the pitch of the wire or the equivalent channel array P. Thus, G.F = (P×L)/($W_0$×T×W). Therefore, the uncertainty of the thermal conductivity can be evaluated by

$$\frac{\delta_\kappa}{\kappa} = \sqrt{\left(\frac{\delta G_s}{G_s}\right)^2 + \left(\frac{\delta P}{P}\right)^2 + \left(\frac{\delta L}{L}\right)^2 + \left(\frac{\delta W_0}{W_0}\right)^2 + \left(\frac{\delta T}{T}\right)^2 + \left(\frac{\delta W}{W}\right)^2}$$

DOI: 10.1038/NNANO.2010.149

The uncertainty of the measured $G_s$ is determined as previously described.

For the NM, $P = 34.6 \pm 1.9$ nm, $L = 7.31 \pm 0.07$ μm, $W_0 = 7.28 \pm 0.04$ μm, $W = 22.81 \pm 2.33$ nm as determined by SEM. $T = 22.3 \pm 1.3$ nm based on AFM measurements at five different positions of the SOI wafer. $G_s = 26.32 \pm 0.51$ nW/K at 250 K. As a result, $\kappa = 1.80 \pm 0.23$ W/m-K.

For the NWA, $P = 34.4 \pm 1.6$ nm, $L = 8.45 \pm 0.13$ μm, $W_0 = 7.71 \pm 0.21$ μm, $W = 28.25 \pm 1.46$ nm, $T = 20.1 \pm 1.2$ nm, $G_s = 56.81 \pm 1.14$ nW/K at 250 K giving $\kappa = 3.40 \pm 0.33$ W/m-K.

**References:**

[31] Tracton, A. A. *Coatings technology handbook*. 62-1 (CRC Press, 2005).

[32] Meng, E., Li, P.-Y. & Tai, Y.-C. Plasma removal of Parylene C. *Journal of Micromechanics and Microengineering* **18**, 045004-045004 (2008).